An Empirical Doubly-Selective Dual-Polarization Vehicular MIMO Channel Model

Guillermo Acosta-Marum, Brett T. Walkenhorst, and Robert J. Baxley
Georgia Tech Research Institute
Atlanta, Georgia 30332-0821
{Guillermo.Acosta-Marum, Brett.Walkenhorst, Bob.Baxley}@gtri.gatech.edu

***Abstract*—To optimally design vehicle-to-vehicle (VTV) communication systems, it is necessary to first fully characterize the response of the communications channel. Significant research attention has been focused on describing channels for various scenarios with both analytical and statistical models based on empirical data (empirical models). This paper extends this field by proffering a doubly selective (i.e., time- and frequency-selective) channel for VTV 2x2 multiple input multiple output (MIMO) systems where the pair of transmit and the pair of receive antennas each have orthogonal polarizations. The proposed empirical model is based on collected channel data in an urban setting and is described by a four-basis function Doppler spectrum for each delay tap. For verification, it is demonstrated that the modeled channel closely matches the collected channel data.**

Keywords- doubly selective wireless propagation models, MIMO, dual polarization, intelligent transportation, mobile-to-mobile WLANs

I. INTRODUCTION

The field of research examining vehicular channel models has grown significantly in recent years as interest has increased in high-speed mobile communication systems for commercial, emergency services, and energy-saving applications. With the development of the 802.11p and the recent push from many sectors, including the U. S. Federal government, for the Smart Grid technology project to include or incorporate intelligent transportation systems (ITS), a proper understanding of wireless communication channels for vehicular applications will be important in aiding system design and standard-validation test-development efforts.

In [1] and [2], we can find recent surveys of previous works related to VTV channel measurements and both theoretical and empirical channel modelling. We may note that geometry-based or theoretical models are more general than statistical models based on empirical data (empirical models) because they can be adapted to different propagation environments or locations, but even though the empirical models are site-specific, they provide advantages that can only come from real channel measurements since they can capture characteristics that are not quantified in a theoretical model. In this paper, we present an empirical model for an urban environment where the transmit (TX) vehicle travelled approximately 100 m ahead of the receive (RX) vehicle at a nominal 35 mph speed. The results we present are for a 2x2 MIMO system using co-located dual-polarized antennas. We selected this type of antenna configuration because of the potential for MIMO capacity and/or diversity enhancement in a compact form factor. This model is easily implemented in currently available channel simulation and emulation tools.

The organization of this paper is as follows: in Section II, we describe the synthesis process of a tap-delay channel, the design and implementation of our channel sounding system, and the development of our modelling process. In Section III, we present the resulting empirical model.

II. MODEL DEVELOPMENT

We usually describe a general or complete characterization of a wireless channel response by three key components: path loss, shadowing, and multipath. The first two components mainly describe large-scale fading. We can loosely assign this large-scale fading to the domain or realm of the automatic gain control (AGC) circuitry of a receiver. The AGC adjusts the receiver gain at a rate slower than the symbol rate yet faster than the fade rate [3]. The third component describes the small-scale fading, which is more in the domain of channel equalization. Multipath happens because objects located around the path of the wireless signal reflect the signal, and some of these reflected waves combine with the original signal at the receiver. Since each of these reflected signals takes a different path, the received signal will be composed of multiple rays, each with a different time of arrival, amplitude and, phase. We can represent the impulse response of a multipath channel as follows:

$$h\left(t,\tau\right)=\sum_{i=1}^{N}c_i\left(t\right)\delta\left(\tau-\tau_i\left(t\right)\right). \tag{1}$$

Equation (1) is a tap-delay line representation where the selection of the number of paths *N* and delay values τ_i for each tap *i* depends upon what we consider or define as a significant level. As indicated, the delay $\tau_i(t)$ and coefficient $c_i(t)$ vary with time, but we usually sample the delay parameter according to what we will define later as T_c, the delay resolution of the model and/or channel sounding or measuring system. For the coefficient $c_i(t)$, we consider a type of model where each of these coefficients is a stochastic time series generated from a random process with Rician or Rayleigh distribution filtered by a Doppler filter whose frequency response is $H_i(f)=\sqrt{S_i(f)}$ where $S_i(f)$ denotes the

Prepared through collaborative participation in the Communications and Networks Consortium sponsored by the U. S. Army Research Laboratory under the Collaborative Technology Alliance Program, Cooperative Agreement DAAD19-01-2-0011. The U. S. Government is authorized to reproduce and distribute reprints for Government purposes notwithstanding any copyright notation thereon.

desired Doppler power spectral density (PSD). Finally, the resulting complex process is scaled to the specified tap power.

We present a summary of the process as follows: we start by generating a time series of a complex random variable

$$r_i(t) = x(t) + jy(t) \tag{2}$$

where $x, y \sim N(0,1)$. The actual implementation of the time series relies on the specifications of the desired system such as available bandwidth and main sampling frequency. We then filter this time series with the Doppler filter to obtain

$$z_i(t) = \int_{-\infty}^{\infty} r_i(\tau) \cdot h_i(t-\tau)\, d\tau \tag{3}$$

where $h_i(t) \leftrightarrow H_i(f)$. Finally, we scale the resulting filtered signal. For a Rayleigh distribution, we have

$$c_i(t) = \sqrt{\mathrm{P}_i}\, z_i(t) \tag{4}$$

where P_i is the desired average power.

RF channel emulators, such as the SPIRENT 5500 [4], and certain communication system simulators, such as Matlab's Simulink, follow this method of wireless channel synthesis, i.e., a random complex number generator followed by a filter with a characteristic spectral shape. In these systems, we can usually find a set of defined spectral shapes. In TABLE I. , we present a list of the spectral shapes that we used in our model development where f_D is the maximum Doppler frequency and f_s is the frequency shift. This list is similar to the set of shapes offered in the aforementioned software simulator [5], but the reader should be aware of the scaling differences between the listed spectra and those of the particular system.

TABLE I. SPECTRAL SHAPES

$S(f)\ \ for - f_D < (f - f_s) < f_D$	**Name of Doppler Spectra**
$\left(1 - \left(\frac{f-f_s}{f_D}\right)^2\right)^{-\frac{1}{2}}$	Classic 6 dB (C6)
$\left(1 - \left(\frac{f-f_s}{f_D}\right)^2\right)^{-\frac{1}{4}}$	Classic 3 dB (C3)
1	Flat (F)
$\left(1 - \left(\frac{f-f_s}{f_D}\right)^2\right)^{\frac{1}{2}}$	Rounded (RI)
$1 - 1.72\left(\frac{f-f_s}{f_D}\right)^2 + 0.785\left(\frac{f-f_s}{f_D}\right)^4$	Rounded IEEE 802.16 (RII)
$3\left(\pi f_D \left(1 + 9\left(\frac{f-f_s}{f_D}\right)^2\right)\right)^{-1}$	Bell (B)
$e^{-\left(\frac{f-f_s}{f_D}\right)^2}\left(\pi f_D\right)^{-\frac{1}{2}}$	Gaussian (G)

A. Sounding System

1) Sounding Waveform Description

We use two time-synchronized waveforms in our sounding system. Following the concept of pulse compression techniques [6], we developed sounding waveforms to measure in the time and frequency domains. After rigorous testing, we decided to use 2047-length Gold sequences for the time domain sounding. We were able to obtain close to 30 dB of cross-correlation separation with these waveforms. We used the preferred polynomials [11 2 0] and [11 8 5 2 0] to generate the set of Gold sequences. For the first transmitter, TX1, we selected the sequence with index one, and for the second transmitter, TX2, we selected the sequence with index ten. Finally, we used both binary sequences to generate binary phase-shift keying (BPSK) symbols.

For the frequency domain, we used a Chirp-like sequence such as (5) to obtain a flat frequency response.

$$s(n) = \cos\left(\tfrac{\pi}{N} n^2\right) + j \sin\left(\tfrac{\pi}{N} n^2\right) \qquad n = 0, \ldots, M-1. \tag{5}$$

The length M is half the size of the number of subcarriers, N, of the OFDM symbol that we used to generate frequency division multiplexing in the sounding waveform as follows: First we obtained the M-sized fast Fourier transform (FFT) $S(k)$ and generated two zero-vectors, $x_1(k)$ and $x_2(k)$ of length $N = 2M$. For TX1, we substituted the sequence $S(k)$ for the even elements of $x_1(k)$, and for TX2, we substituted the sequence $-S(k)^*$ for the odd elements of $x_2(k)$. Since a BPSK symbol generates a double-sided RF spectrum, its time-domain signal requires two "chip" T_c time-periods per symbol; therefore, we need to apply rectangular pulse shaping to the Gold sequences. This chip period is the elementary time-period of the baseband recorded complex data symbols that we process with Matlab. Since an OFDM symbol generates a complex RF spectrum, we need only one T_c time-period for each element of $x_{1,2}(k)$. Before the digital-to-analog conversion, we still have to oversample the signal by a factor of two, i.e., T_c=$2T_s$ where T_s is the sampling-period. Since the Gold sequence is a time-domain signal, we just hold each T_c for $2T_s$, but for the frequency-domain signals, $x_{1,2}(k)$, we insert a block of zeros between the upper and lower sidebands. To generate the time-domain OFDM symbol, we apply an inverse FFT (IFFT) to these oversampled signals, and since it is OFDM, we use a cyclic prefix (CP) to help us in the synchronization process. In this case, we used a ¼ length CP. Finally, to help with synchronization and to measure the signal-to-noise ratio (SNR), we introduce two zero vectors with the same length as the OFDM symbol before and after it. The final signal consists of a 2047-length Gold sequence, first zero vector, OFDM symbol, and second zero vector. Therefore, the total length of each of the sounding waveforms is 10,748 T_s, and since our sampling frequency is 72 MHz, the total period of the complete sounding signal is $T_D = 149.28\,\mu s$.

2) Sounding System Specifications

Our sounding system can measure time- and frequency-selective channels; therefore, its purpose is to measure Doppler-delay profiles described by the scattering function

$S(f,\tau)$. Starting with a sampling frequency of 72 MHz, which translates into a 36 MHz RF bandwidth, we obtain a period of $T_c = 1/72MHz \cong 28ns$. For each repetition of a sounding wave, we obtain two measured channel impulse responses $h_{Gold}(t,\tau_{Gold})$ and $h_{OFDM}(t,\tau_{OFDM})$. We obtain the former by filtering the recorded baseband complex symbols using the elements of the original sequence as the coefficients of an FIR filter. The output of this filter is the h_{Gold} channel impulse response. For the latter, we used the correlation result of the time-domain sequence to localize the position of the OFDM symbol. Once we have synchronized the OFDM symbol, we remove the CP, apply an FFT, and select the corresponding subcarriers to obtain the recorded Chirp-like sequence. Dividing it by the original signal, we obtain the channel transfer function, and the IFFT of this result is the h_{OFDM} channel impulse response. We can also use the obtained synchronization to separate two noise vectors generated by the original zero vectors.

As mentioned in the previous section, the Gold-sequences require two chip periods per symbol; therefore, their delay resolution is twice the time of the frequency-domain delay resolution: $\tau_{Gold} = 2 \cdot \tau_{OFDM}$. The delay measurement ranges for the time and frequency-domain signals are $2047 \cdot \tau_{Gold} = 114.632\mu s$ and $256 \cdot \tau_{OFDM} = 7{,}168\mu s$ respectively. Summarizing, with the frequency-domain signal we can differentiate multipath with distance difference greater than 8.4 meters up to 17.194 km. For Doppler frequency measurements, the measurement range depends on the sounding wave repetition rate. In our case, the Doppler frequency range is $f_{D\max} = \pm 1/2T_D = 3{,}350Hz$, which for the system's carrier frequency of 2.435 GHz corresponds to a maximum Doppler velocity of 412 m/s or 923 mph. Finally, the system is capable of recording approximately 35,500 continuous impulse responses for a total recording time of 5.3 seconds. With these 5.3 seconds, we can obtain Doppler frequency resolution of 0.17 Hz.

3) System and Measurement Campaign Descriptions

We refer the reader to [7] where we present detailed description of the system utilized for the channel-sounding campaign. For this particular set of channel-sounding measurements, we used SuperPass™ 2.4 GHz Dual Polarized Omni-Directional antennas and Empower RF power amplifiers with a transmitting power of +30 dBm. We took the measurements in an urban environment around the Georgia Tech campus. The vehicle speeds ranged from 25 to 35 mph and the separation between vehicles averaged 100 m.

B. Modelling Approach

1) Overall Scattering Function

For the model development, we use the resulting 2x2 MIMO channel impulse response matrix

$$\mathbf{h}_{OFDM2\times2} = \begin{bmatrix} \mathbf{h}_{OFDM\mathbf{VV}} & \mathbf{h}_{OFDM\mathbf{VH}} \\ \mathbf{h}_{OFDM\mathbf{HV}} & \mathbf{h}_{OFDM\mathbf{HH}} \end{bmatrix} = \begin{bmatrix} \mathbf{h}_{11} & \mathbf{h}_{12} \\ \mathbf{h}_{21} & \mathbf{h}_{22} \end{bmatrix} \quad (6)$$

where the overall size of the matrix is 2x2x35,500x256 since each element of the matrix is a 256 size row vector and there are 35,500 vectors. As indicated in (6), we will refer to the matrix elements by their numerical indices We averaged the magnitude squared of each element of each impulse response matrix down the columns to generate an overall power delay profile (PDP). We applied a threshold of approximately 25 dB relative to the highest peak of the four PDPs to eliminate noise effects in the PDPs, and we set the samples below the threshold to zero. The bins with power greater than this threshold are called the significant taps of the overall PDP, and they become the taps of the final model for the particular site. This significant-tap assignment fixes the power and number of taps for each MIMO stream.

Using the process detailed in [8], we obtained the power spectral density (PSD) for each selected significant tap in each matrix. In Fig. 1, we present the resulting 2x2 MIMO empirical scattering function (SF) $S(f,\tau)$. As we can observe, $.h_{11}.$ is the strongest or dominant stream. All the selected taps are scaled equally such that this dominant tap is normalized. We can also observe a narrow peak in most of the spectra up to the third significant tap or bin. As in [9] and many other publications related to empirical channel modelling, we used the moment method [10] to estimate the K-factor, that is, the power ratio between the fixed and fluctuating components, but on this occasion, we did not find a significant K-factor for the complete time series. Therefore, the model in this paper contains only Rayleigh distributions. We applied the moment method to different time windows, and we found significant K-factor values. In essence, we believe that one of the main characteristics of a VTV channel resides in the non-constant characteristic of the K-factor, which current software and channel emulation systems do not implement. Another consideration of these systems is that they require fixed PSDs, but as indicated in [11], another important characteristic should be a time-variant PSD.

2) Spectral Fitting

Following the technique described in [9] we proceeded to fit the 30 PSDs of the obtained SF using only spectral shapes from the list in Table I. For this purpose, we constructed a tap from several paths. We define a path as a single complex random process filtered by only one of the spectral shapes listed. Since none of the listed spectral shapes is sufficient to describe most of the resulting measured Doppler spectra, we construct a customized Doppler spectrum that fits better by superimposing several paths with the same delay. The model we are presenting is more oriented towards simulation synthesis rather than hardware emulation where the number of available paths is usually six or twelve. From previous experience, we found that three paths is a good trade-off between complexity and accuracy for each tap. We optimized each tap spectrum fit by taking the best of five runs of a genetic algorithm. The cost function used in the genetic algorithm for selecting the best of the five was the integrated weighted difference between the measured spectrum and the customized spectrum. The weighting function was $(f - f_{peak})^2$, where f_{peak} is the frequency of the peak (usually very well defined) of the spectrum of the first (and strongest) tap. It is assumed that f_{peak} is the recovered carrier frequency in the receiver. The cost function ensures that the inter-carrier interference (ICI) that would be produced by the customized spectrum in an

OFDM receiver is as close as possible to the ICI produced by the measured spectrum [12]. The customized Doppler spectrum for each tap is constrained to have the same total power (i.e. same area in a non-dB plot) as the measured Doppler spectrum, so that the power delay profile is preserved.

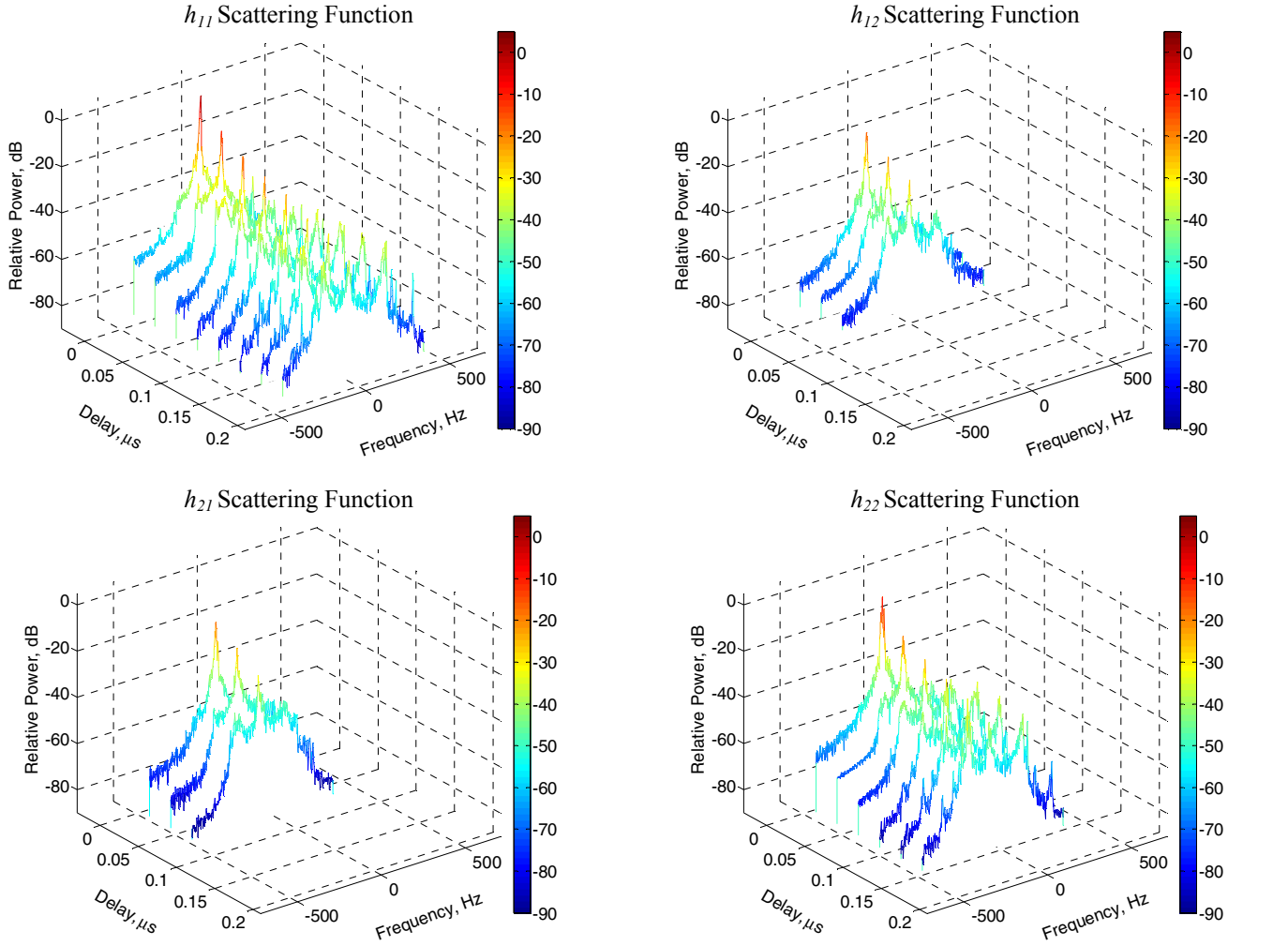

Figure 1. MIMO 2x2 Measured Scattering Function $S(f,\tau)$

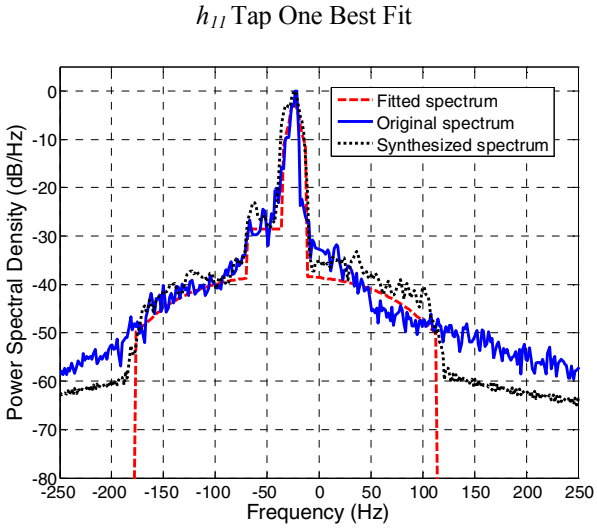

Figure 2. PSD fitting and synthesis using three spectral shapes example

In Fig. 2, we present an example of the fitting of the first tap of h_{11} where the blue solid line is the original measured spectrum, the red dashed line is the combination of three optimally scaled and fitted spectral shapes from Table I, and the black dotted line is the measured or sounded spectrum of the software synthesized tap model. We performed the software synthesis by a direct implementation of the taped-delay synthesis process.

III. MODEL DESCRIPTION

In Table II, we present the empirical model parameters. Each set of the parameters "Frequency Shift," "Fading Doppler," and "Fading Spectral Shape" describes a single Doppler spectrum. Respectively, these parameters mean center (baseband) frequency, frequency half-width of the spectrum, and the basic shape of the spectrum selected only from Table I. The repeated numbers in the cells of "Tap No." column indicate the required number of paths to create the composite spectrum. The corresponding combined path powers provide an

accurate approximation of the tap power as shown in Fig. 2. Whenever we indicate a multi-element vector in one of the cells, the i^{th} element corresponds to the corresponding MIMO stream as indicated in the notes below.

IV. Conclusion

In this paper, we presented the development of an empirically-derived channel model suitable for simulation or emulation. This development included a description of the design and implementation of the MIMO channel sounding system used, which is capable of capturing fine resolution delay and Doppler characteristics of a wideband VTV channel. We also included a description of a tap-delay channel synthesis to allow the implementation of the presented model.

Disclaimer

TABLE II. 2x2 MIMO VTV CHANNEL MODEL FOR DUAL-POLARIZED COLLOCATED ANTENNAS

Tap No.	Path No.	Relative Path Loss P (dB)	Delay Value τ (ns)	Frequency Shift f_s (Hz)	Fading Doppler f_D (Hz)	Fading Spectral Shape $S(f)$
[1, 1, 1, 1]	1	[8.8, -6.3, -11.2, -4.7]	0	[-24, -24, -25, -29,]	[12, 11, 13, 11]	[B, B, B, G]
[1, 1, 1, 1]	2	[-29.0, -42.6, -30.0, -20.3]	0	[-44, -34, -25, -32]	[26, 87, 59, 60]	[F, RII, RII, G]
[1, 1, 1, 1]	3	[-38.2, -52.7, -32.8, -29.7]	0	[-32, -32, 11, 0]	[146, 197, 167, 193]	[RII, RII, G, G]
[2, 2, 2, 2]	4	[-14.1, -27.2, -28.1, -22.9]	28	[-26, -21, -27, -27]	[13, 18, 17, 12]	[RII, RII, RII, RI]
[2, 2, 2, 2]	5	[-22.4, -40.1, -37.2, -24.6]	28	[39, 26, 8, -51]	[170, 138, 193, 80]	[G, G, G, G]
[2, 2, 2, 2]	6	[-23.2, -43.8, -47.4, -45.0]	28	[-73, -46, -24, -4]	[110, 122, 84, 192]	[G, RII, B, B]
[3, 3, 3, 3]	7	[-22.4, -32.9, -31.3, -30.1]	56	[-26, -20, -23, -21]	[16, 25, 22, 21]	[RI, RII, B, RII]
[3, 3, 3, 3]	8	[-35.2., -34.8, -46.1, -44.3]	56	[-83, -2, 4, -8]	[102, 173, 202, 170]	[F, G, RI, C3]
[3, 3, 3, 3]	9	[-46.7, -34.9, -59.6, -48.3]	56	[5, -80, 38, -15]	[165, 113, 261, 280]	[F, G, RII, G]
[4, n/a, n/a, 4]	10	[-26.3, n/a, n/a, -42.6]	84	[-18, n/a, n/a, 50]	[22, n/a, n/a, 112]	[RI, n/a, n/a, C3]
[4, n/a, n/a, 4]	11	[-43.6, n/a, n/a, -47.8]	84	[-83, n/a, n/a, -5]	[95, n/a, n/a, 172]	[C3, n/a, n/a, C3]
[4, n/a, n/a, 4]	12	[-48.2, n/a, n/a, -53.4]	84	[-2, n/a, n/a, 15]	[179, n/a, n/a, 199]	[RI, n/a, n/a, RII]
[5, n/a, n/a, 5]	13	[-26.2, n/a, n/a, -34.7]	112	[-27, n/a, n/a, -28]	[43, n/a, n/a, 32]	[B, n/a, n/a, B]
[5, n/a, n/a, 5]	14	[-39.8, n/a, n/a, -43.4]	112	[-15, n/a, n/a, 95]	[182, n/a, n/a, 336]	[C3, n/a, n/a, B]
[5, n/a, n/a, 5]	15	[-49.3, n/a, n/a, -46.4]	112	[-8, n/a, n/a, -3]	[249, n/a, n/a, 178]	[RI, n/a, n/a, C6]
[6, n/a, n/a, 6]	16	[-41.7, n/a, n/a, -43.0]	140	[-92, n/a, n/a, -95]	[109, n/a, n/a, 57]	[C3, n/a, n/a, C6]
[6, n/a, n/a, 6]	17	[-45.8, n/a, n/a, -52.9]	140	[54, n/a, n/a, 5]	[145, n/a, n/a, 180]	[C6, n/a, n/a, F]
[6, n/a, n/a, 6]	18	[-65.4, n/a, n/a, -56.6]	140	[-75, n/a, n/a, -84]	[294, n/a, n/a, 123]	[RII, n/a, n/a, C3]
[7, n/a, n/a, n/a]	19	[-42.0, n/a, n/a, n/a]	168	[-96, n/a, n/a, n/a]	[95, n/a, n/a, n/a]	[C6, n/a, n/a, n/a]
[7, n/a, n/a, n/a]	20	[-48.5, n/a, n/a, n/a]	168	[5, n/a, n/a, n/a]	[185, n/a, n/a, n/a]	[C6, n/a, n/a, n/a]
[7, n/a, n/a, n/a]	21	[-64.5, n/a, n/a, n/a]	168	[45, n/a, n/a, n/a]	[345, n/a, n/a, n/a]	[RII, n/a, n/a, n/a]
[8, n/a, n/a, n/a]	22	[-45.9, n/a, n/a, n/a]	196	[1, n/a, n/a, n/a]	[194, n/a, n/a, n/a]	[C6, n/a, n/a, n/a]
[8, n/a, n/a, n/a]	23	[-48.3, n/a, n/a, n/a]	196	[-54, n/a, n/a, n/a]	[286, n/a, n/a, n/a]	[G, n/a, n/a, n/a]
[8, n/a, n/a, n/a]	24	[-56.0, n/a, n/a, n/a]	196	[-84, n/a, n/a, n/a]	[142, n/a, n/a, n/a]	[C6, n/a, n/a, n/a]

1. Data vector format: [h_{11} (VV), h_{12} (VH), h_{21} (HV), h_{22} (HH),]
2. Relative Path Loss values should be scaled according to the power of the spectral shape of the synthesis system
3. Spectral shapes are Classic 6 dB (C6), Classic 3 dB (C3), Flat (F), Round (RI), Round 802.15 (RII), Bell (B), and Gaussian (G)
4. n/a means not-applicable

References

[1] J. A. F. Molisch, F. Tufvesson, J. Karedal, and C. Mecklenbrauker, "Propagation aspects of vehicle-to-vehicle communications – an overview," Proc. IEEE Radio and Wireless Symposium (RWS 2009), pp. 179-182, January 2009.

[2] A. F. Molisch, F. Tufvesson, J. Karedal, and C. Mecklenbrauker, "A survey on vehicle-to-vehicle propagation channels," *IEEE Wireless Communications*, vol. 16, no. 6, pp. 12-22, December 2009.

[3] J. S. Seybold, Introduction to RF Propagation, Hoboken, NJ, John Wiley & Sons, 2005

[4] Spirent Communications SR5500 Wireless Channel Emulator Operations Manual. www.spirentcom.com

[5] Iskander, Cyril-Daniel, *A MATLAB-based Object-Oriented Approach to Multipath Fading Channel Simulation*, a MATLAB Central submission available from www.mathworks.com.

[6] J. D. Parsons, D. A. Demery, and A.M.D. Turkmani, "*Sounding techniques for wideband mobile radio channels: a review*," *IEE Proceedings*, vol. 138, no. 5, pp. 437-446, 1991.

[7] A. G. Zajić, G. L. Stüber, T. G. Pratt, and S. T. Nguyen, "*Wideband MIMO mobile-to-mobile channels: geometry-based statistical modeling with experimental verification,*" IEEE Trans on Vehicular Technology , vol. 58, no. 2 pp. 517-534, February 2009.

[8] G. Acosta and M. A. Ingram, "Model development for the wideband vehicle-to-vehicle 2.4 GHz channel," Proc. IEEE Wireless Communications & Networking Conference (WCNC 2006), Las Vegas, NV, 3-6 April 2006.

[9] G. Acosta-Marum and M. A. Ingram, "Doubly selective vehicle-to-vehicle channel measurements and modeling at 5.9 GHz," in Proc. Wireless Personal Multimedia Communications Conference (WPMC 2006).

[10] L. J. Greenstein, D. G. Michelson, and V. Erceg, "Moment-method estimation of the Ricean *K*-factor," in *IEEE Communications Letters*, vol. 3, No. 6, pp. 175-176, June 1999.

[11] A. Paier, et al. "Non-WSSUS vehicular channel characterization in highway and urban scenarios at 5.2 GHz using the local scattering function," in International Workshop on Smart Antennas, (WSA 2008), Darmstadt, Germany, Feb. 2008.

[12] X. Cai and G.B. Giannakis, "*Bounding performance and suppressing intercarrier interference in wireless mobile OFDM*," IEEE Trans. Comm. Vol. 51, No. 12, December 2003.